Desalination and Water Treatment
www.deswater.com

doi: 10.5004/dwt.2019.24405

163 (2019) 166–178
September

Electrostatic attraction based on N-rich dendrimer amines grafted onto graphene oxide for the removal of chromium(VI) from aqueous solution

Xuezhen Feng[a], Fangli Liao[b,*], Zijie Guo[a], Mingyue Peng[a]

[a]*School of Chemistry and Chemical Engineering, Central South University, Changsha 410083, China, emails: fxz867545880@csu.edu.cn (X. Feng), 943379253@163.com (Z. Guo), 2361325106@qq.com (M. Peng)*
[b]*School of Chemistry and Materials Engineering, Huizhou University, Huizhou 516007, China, email: 1628640576@qq.com*

Received 26 November 2018; Accepted 10 May 2019

ABSTRACT

Chromium(VI) pollution has aroused great attention due to its potential toxicity to human health. In this article, N-rich dendrimer amines grafted onto graphene oxide through cyanuric chloride and diethylenetriamine (GO/CC-DETA) was constructed for chromium(VI) removal from aqueous solution. The adsorption studies for optimum conditions, such as molar ratio of DETA to CC, pH, contact time, and temperature, were proceeded in batch mode. Kinetic and thermodynamic study of adsorption were also explored, where the Langmuir isotherm and pseudo-second-order kinetics fitted the best, and the obtained monolayer adsorption capacity could reach 295.9 mg g^{-1}. The main adsorption mechanism of GO/CC-DETA toward Cr(VI) was proved to be electrostatic interaction. Practical desorption–regeneration results showed that the adsorption capacity could remain relatively stable after several times of usage.

Keywords: Chromium(VI); N-rich dendrimer amine; Graphene oxide; Adsorption; Electrostatic interaction

1. Introduction

With the further urbanization of society in recent few decades, plenty of chromium-containing wastes have been left behind due to the relocation of many industrial manufactures, such as electroplating, chromium salt production, and printing and dyeing. These have caused serious Cr(VI) pollution in groundwater. Chromium is a potentially toxic heavy metal without any essential metabolic function in plants and is easily retained in the root tissues [1,2], so it can accumulate in crops, and extend health risks to humans via food chain. In fact, the concentration of chromium uptake by Cr-polluted edible plants can exceed the maximum permissible limits and cause numerous harms to our body [3]. Moreover, chromium is categorized as No. 1 carcinogen according to the International Agency for Research on Cancer and the National Toxicology Program [4]. Both direct and indirect chromium intake from chromium-containing groundwater has intensified the severity of environmental and health problem.

Actually, unlike other toxic heavy metal cations, chromium, with two main states of trivalent and hexavalent, mainly exists as more hypertoxic and negative chromates. Techniques reported for chromium metals removal include ions exchange [5,6], adsorption [7,8], chemical precipitation [8,9], membrane filtration [9,10], electrodialysis [11], photocatalysis [12], etc. Almost all methods have merits and limitations, such as high cost, limited application and serious secondary pollution generation. However, adsorption is proved to be a relatively economic and effective method for hexavalent chromium removal from wastewater.

Many researchers have delved into adsorbents with high adsorption property, low cost, renewable performance, and ease of access for practical application. Numerous materials have been employed, including activated carbon [10,11], zeolite [13], biomaterials [14–16], kaolinite [17,18],

* Corresponding author.

manganese oxide [19], resins [20], metal organic frame material [21,22], etc. Graphene oxide (GO) is an up-to-the-moment and two-dimensional inorganic carbon nanomaterial developed in last few decades. It owns high surface area and rich functional groups on the surface. Whereas Cr(VI) exists in the form of negative acid ions ($Cr_2O_7^{2-}$, CrO_4^{2-} and $HCrO_4^-$), thus novel GO-based materials with positive charge and high affinity for anions should be explored. Nitrogen-containing compounds are prone to protonation under acidic conditions and have strong electrostatic attraction to metal anions. Based on previous works, aminated graphene oxide has shown great adsorption capacity toward hexavalent chromium [23–25]. Diethylenetriamine (DETA) is an organic polyamine molecule, and has been applied in hexavalent chromium removal from wastewater, such as diethylenetriamine grafted glycidyl methacrylate based copolymers [26], diethylenetriamine modified magnetic chitosan [27], diethylenetriamine-assisted synthesis of amino-rich hydrothermal carbon-coated electrospun polyacrylonitrile fiber, etc. [28].

In this study, diethylenetriamine was chosen in collaboration with cross linker cyanogen chloride to prepare N-rich dendrimer amine grafted graphene oxide materials for achieving higher adsorption capacity for Cr(VI). Fourier transform infrared spectroscopy (FTIR), Raman spectra (Raman), X-ray photoelectron spectroscopy (XPS), field emission scanning electron microscope (FE-SEM), high-resolution transmission electron microscope (HR-TEM) were used to characterize the prepared GO/CC-DETA and analyze the adsorption mechanism. Simultaneously, a synergistic action of cyanuric chloride (CC) and diethylenetriamine (DETA) was discussed in detail. The influences of molar ratio, pH, contact time, temperature and cycle number of the adsorption process were studied. The as-prepared composite (GO/CC-DETA) showed good adsorption capacity toward Cr(VI).

2. Experimental

2.1. Reagents

Natural flaky graphite (100 mesh, purity > 95%) was purchased from Shenzhen Nanotech Port Co. Ltd. (Guangdong, China). Hydrochloric acid (HCl, 37 wt.%) and sulfuric acid (H_2SO_4, 98%) were obtained from Chengdu Cologne Chemicals Co. Ltd. (Chengdu, China), and hydrogen peroxide (H_2O_2, 30 wt.%) and phosphoric acid (H_3PO_4, 98%) were from National Group Chemical Reagent Co. Ltd. (Shanghai, China). Potassium permanganate ($KMnO_4$) was purchased from Xirong Science Co. (Shantou, Guangdong, China), sodium hydroxide was obtained from Beijing Chemical Factory Ltd. (Beijing, China). Diethylenetriamine (DETA) was obtained from Tianjin Fuchen Chemical Reagent Technologies Co. Ltd. (Tianjing, China). Cyanuric chloride (CC) was purchased from Aladdin Industrial Corporation (Shanghai, China). Metal salt $K_2Cr_2O_7$ was used as source for Cr(VI). All chemicals were of analytical grade and used as received without any further treatment. Ultra-pure water was produced using a Milli-Q water purification system (Millipore, Milford, MA).

2.2. Synthesis of N-rich dendrimer aminated graphene oxide (GO/CC-DETA)

2.2.1. Preparation of graphene oxide aqueous dispersion

A nitration mixture of phosphoric acid (4 mL) and sulfuric acid (36 mL) was prepared ahead, and in cold storage. To a mixture of potassium permanganate (1.5 g) and crystalline flake graphite (0.3 g), the preparation solution was dropwise added along the side in an ice-water bath. After stirring for 12 h under 50°C, the oxidizing reaction was finished, and ice cubes were used to dilute the solution and potassium permanganate residue was reduced by hydrogen peroxide. Subsequently, the yellow graphene oxide aqueous dispersion was purified through multiple pickling and ultrapure water washing.

2.2.2. Decoration of N-rich dendrimer amines onto graphene oxide

First, required cyanuric chloride (CC) was dissolved in DMF (1 mL), and the solution was added in 2.5 mL of diethylenetriamine (DETA). After ultrasonic treatment for 2 h and refrigerated overnight, N-rich dendrimer amines were obtained. Then, it was mixed with 5 mL of graphene oxide aqueous dispersion (5 mg mL^{-1}) and diluted to 20 mL. After ultrasonic treatment for 30 min, the mixture was transferred to a Teflon-lined stainless-steel autoclave for hydrothermal reaction at 120°C for 4 h. Then washed thoroughly with ultra-pure water and dried by freeze-drying, N-rich dendrimer aminated graphene oxide (GO/CC-DETA) was obtained. The schematic illustration of fabrication process and formation mechanism of GO/CC-DETA nanocomposites is presented in Fig. 1.

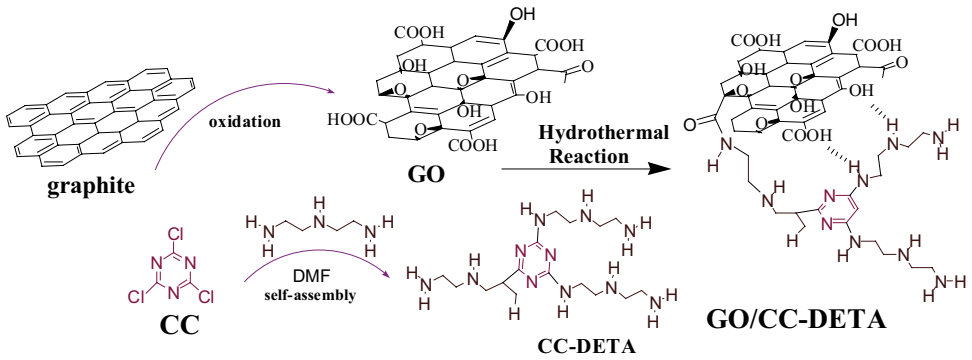

Fig. 1. Schematic illustration of fabrication process and formation mechanism of GO/CC-DETA nanocomposites.

2.3. Characterization of GO/CC-DETA nanocomposites

FTIR spectrometer (PerkinElmer Instruments Co. Ltd., USA), Raman spectra (Renishaw micro-Raman system 2000 spectrometer, London, UK), XPS (ESCALab220i-XL, VG Scientific, Waltham, MA, USA), scanning electron microscopy (SEM: JEOL, JSM-6360LV, Japan) and HR-TEM (Talos F200i for Materials Science) were used for illustrating the GO/CC-DETA nanocomposites.

2.4. Batch adsorption experimental procedures

Potassium dichromate was selected as the representative of toxic Cr(VI) compound in the wastewater, and Cr(VI)-containing wastewater (1 g L^{-1}) was prepared and stored at room temperature for diluting into a standard series concentrations. Adsorption capacity of the GO/CC-DETA nanocomposites toward Cr(VI) was measured as follows: a certain amount of prepared GO/CC-DETA nanocomposites (5 mg) and known initial concentration of Cr(VI)-containing standard solution (25 mL) were mixed and shaken for a certain time, the residual Cr(VI) in the solution was determined by inductive coupled plasma atomic emission spectrometer (ICP-AES). The adsorption capacity was calculated based on the Cr(VI) ions concentration difference before and after adsorption, and the formula is as follows:

$$q_e = \frac{C_0 - C_e}{m} \times V \quad (1)$$

where C_0 and C_e (mg L^{-1}) were the initial and residual concentrations of Cr(VI), m (mg) was the mass of the adsorbent, V (mL) was the volume of the solution, and q_e (mg g^{-1}) was the adsorption capacity of absorbent toward Cr(VI).

Through altering the initial concentration, pH, oscillation temperature and time, the influences of these factors on the adsorption of Cr(VI) were studied.

2.5. Desorption and regeneration experiment

Desorption and regeneration experiments were directly controlled by the solution pH. Desorption of Cr(VI) was performed by applying negative potential on GO/CC-DETA in 0.1 mol L^{-1} NaOH + 0.1 mol L^{-1} NaCl solution. The Cr-load materials were rinsed in the alkaline eluent overnight, and the process was repeated for three times. Regeneration of the sorption sites needed to stir GO/CC-DETA in 0.1 mol L^{-1} HCl solution, where the process was also repeated for three times.

3. Results and discussion

3.1. Characterization of samples

Fig. 2a shows the FTIR spectra of GO, RGO, GO/DETA, GO/CC-DETA, displaying the slight changes triggered by grafting N-rich dendrimer amines. It was obvious that the broad bands at around 3,425 cm^{-1} (O–H stretching vibration of the carboxylic acids groups), peaks located at 1,626 cm^{-1} (aromatic C=C) and the peaks located at 1,149 cm^{-1} (bending vibration in C–H plane, stretching vibration of C–O and vibration of C–C single bond skeleton) were preferably reserved. There were slight increases at 2,842 and 2,949 cm^{-1} which

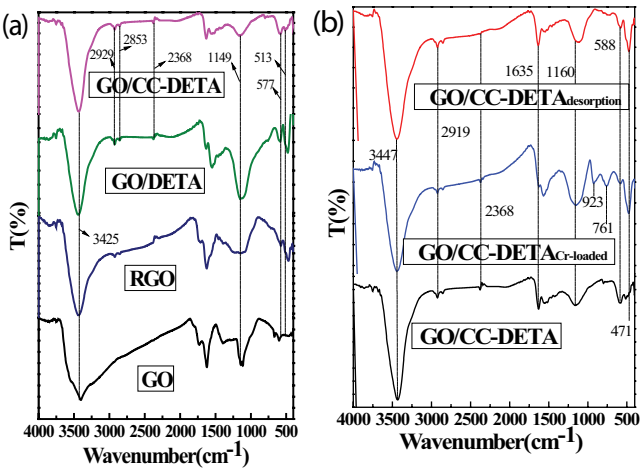

Fig. 2. FTIR analysis: (a) FTIR spectra of GO, RGO, GO/DETA, GO/CC-DETA and (b) FTIR spectra of GO/CC-DETA, GO/CC-DETA$_{Cr\text{-}loaded}$, GO/CC-DETA$_{desorption}$.

were assignable to asymmetric stretching and symmetric stretching modes of CH_2 on the DETA chains. With some carbonyl moieties converting into amides, the new absorption peak at 1,560 cm^{-1} (NH_2 in-plane deformation vibration) appeared on the FTIR spectra of GO/DETA, GO/CC-DETA, and slight peak shifts around 513 and 588 cm^{-1} (N–H bond stretching) were annotated [27–29].

The D band of Raman spectrum of graphene indicates the properties of the graphene edge, such as defects, vacancies, etc., and the G band represents the first-order scattering E_{2g} vibration mode, mainly used to characterize the sp^2 bond structure of carbon. The I_D/I_G is a measure of disordered graphite. In general, the larger the ratio of I_D/I_G, the more defects in C atomic crystals. Fig. 3 presents the Raman spectra of GO, RGO, GO/DETA, and GO/CC-DETA, where the locations at 1,326 (D band) and 1,582 cm^{-1} (G band) remained relatively stable. And the increasing ratio (I_D/I_G) of GO (0.793), RGO (1.196), GO/DETA (1.345), GO/CC-DETA (1.380) revealed that higher disorder of graphene layers took place during the functionalization process [30].

Survey spectra (Fig. 4a) and N1s (Fig. 4b) of XPS data of GO/CC-DETA are presented. The C:O:N ratio of GO/CC-DETA was 78:8:14. The existence of 13.7% nitrogen atom indicated the grafting of N-rich dendrimer amines. N1s peak-differentiation-imitating analysis (Fig. 4b) of GO/CC-DETA corresponded, respectively, to –CO–NH (398.3 eV), –N–H (399.3 eV), C=N– (400.2 eV) groups. The above findings proved the existence of N-rich dendrimer amines on GO/CC-DETA.

FE-SEM (Fig. 5) was used to illustrate the effects generated by the modification on the morphology of materials. Fig. 5a indicates that GO nanosheets presented a smooth single-layer structure with some curved edges. However, carbon nanosheets crimped and draped at an increasing extent in sequence of GO (a), RGO (b), GO/DETA (c), GO/CC-DETA (d) [23].

High-resolution TEM images (Figs. 6a–c) are presented to give further information on the morphology. It was obvious that the graphene lamellar structure was well preserved. Meanwhile, the elemental mapping images (Fig. 6d) of GO/CC-DETA indicate intuitively the presence of primary amine

groups from DETA and elemental distribution analysis of C, N, O in the material was a good response to the XPS and FTIR analysis. It can be concluded that graphene oxide nanoparticles were successfully functionalized with N-rich dendrimer amines.

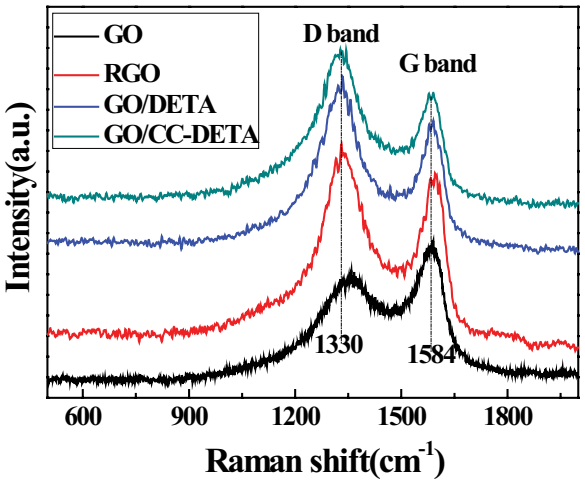

Fig. 3. Raman spectra of GO, RGO, GO/DETA, and GO/CC-DETA.

3.2. Adsorption results

The adsorption capacities of GO, GO/DETA, GO/CC-DETA toward Cr(VI) solution of different concentrations are displayed in Fig. 7. And the results illustrated GO/CC-DETA with N-rich dendrimer amines had the better adsorption capacity toward Cr(VI) than those of GO and GO/DETA. Fig. 8 shows the effect of the molar ratios of diethylenetriamine (DETA) to cyanuric chloride (CC) on the adsorption of Cr(VI) by GO/CC-DETA, where the 1:2.5 exhibited the best adsorptive performance. And the effects of the pH values (Fig. 8), vibration time (Fig. 9) and temperature (Fig. 10) were also explored for follow-up mechanism analysis. It was found that the adsorption equilibrium was reached in about 80 min, and acidic and hyperthermal surrounding favored the adsorption process.

3.3. Adsorption kinetics

Adsorption kinetics in wastewater treatment is important as it provides valuable insights into the paths and mechanism of adsorption reaction. It is also important to predict the rate at which Cr(VI) is removed from aqueous solutions for the design of appropriate sorption treatment. In addition, the kinetics describe the solute uptake rate which

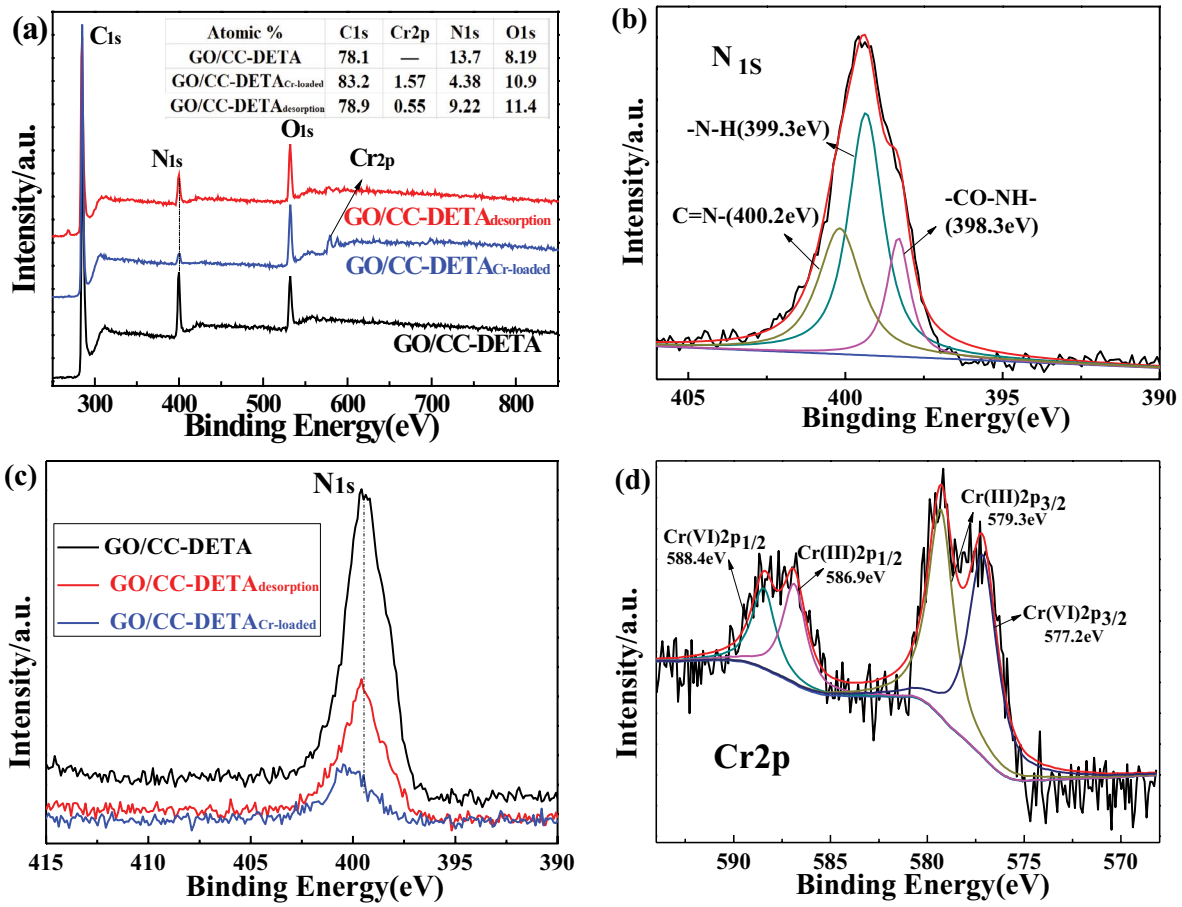

Fig. 4. XPS spectra analysis: (a) Survey spectra of XPS data of GO/CC-DETA$_{desorption}$, GO/CC-DETA$_{Cr\text{-}loaded}$, GO/CC-DETA, (b) N1s XPS spectra of GO/CC-DETA, (c) N1s comparison of GO/CC-DETA$_{desorption}$, GO/CC-DETA$_{Cr\text{-}loaded}$, GO/CC-DETA, and (d) Cr2p XPS spectra of GO/CC-DETA$_{Cr\text{-}loaded.}$

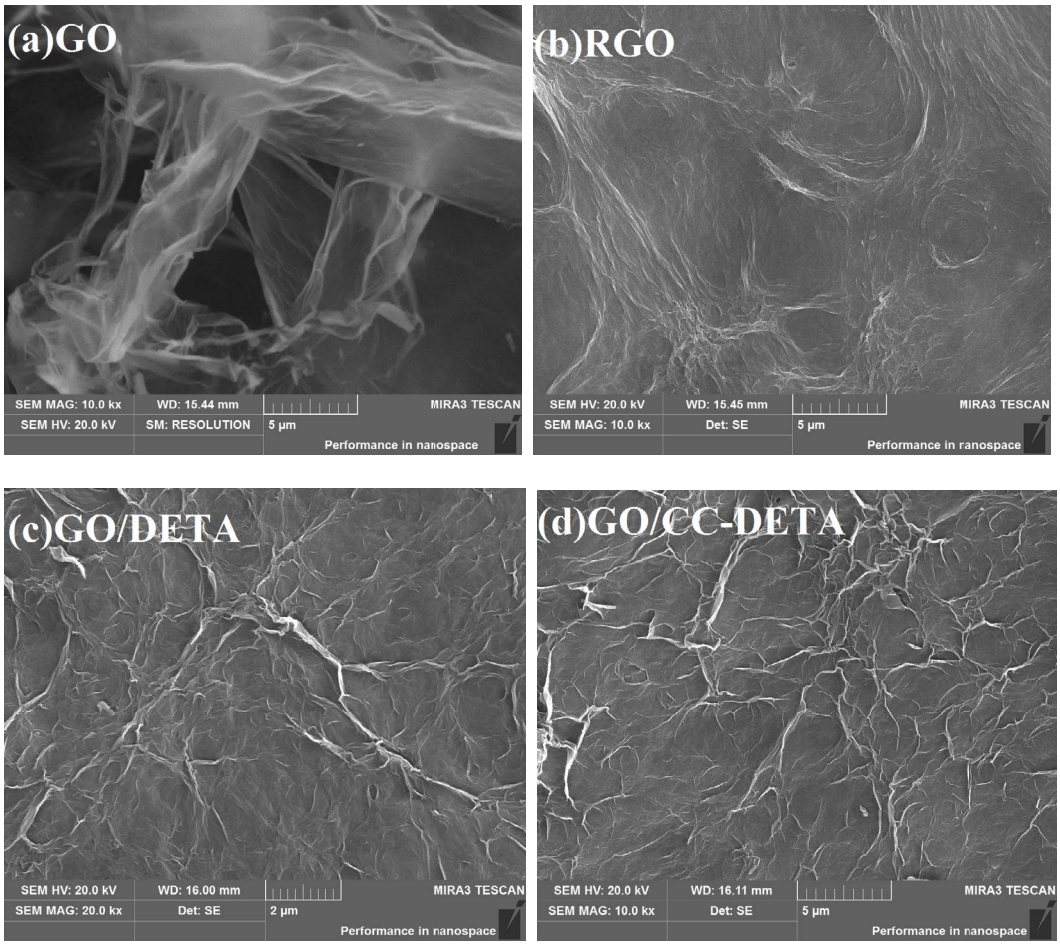

Fig. 5. SEM images: (a) GO, (b) RGO, (c) GO/DETA, and (d) GO/CC-DETA.

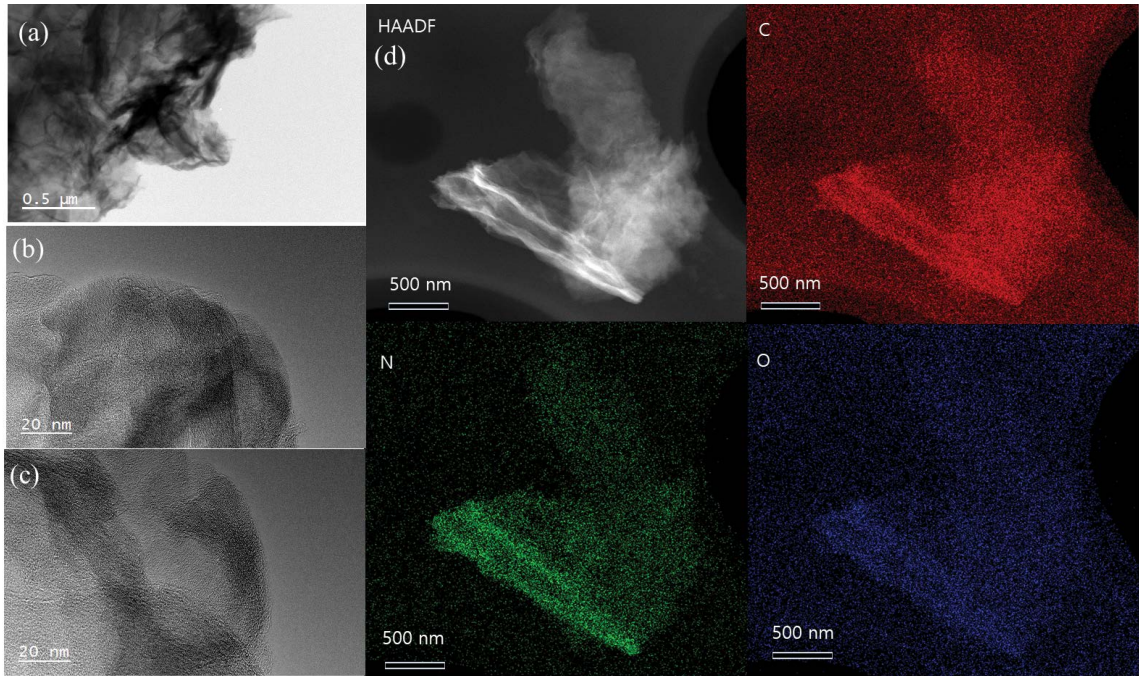

Fig. 6. High resolution TEM images (a–c) and elemental mapping images (d) of GO/CC-DETA.

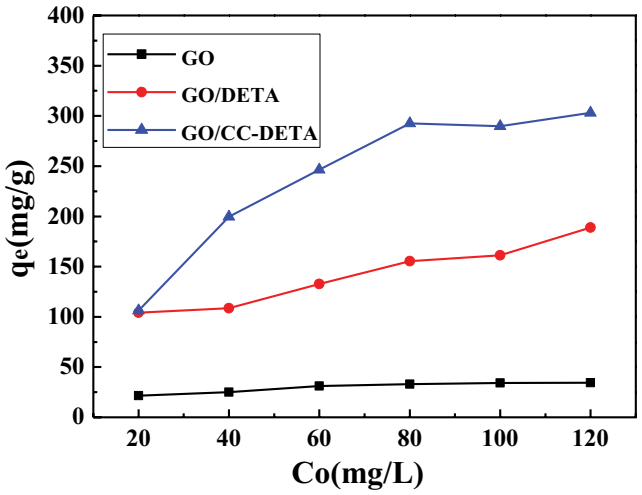

Fig. 7. Adsorption capacities of different materials toward Cr(VI) solution with different concentrations.

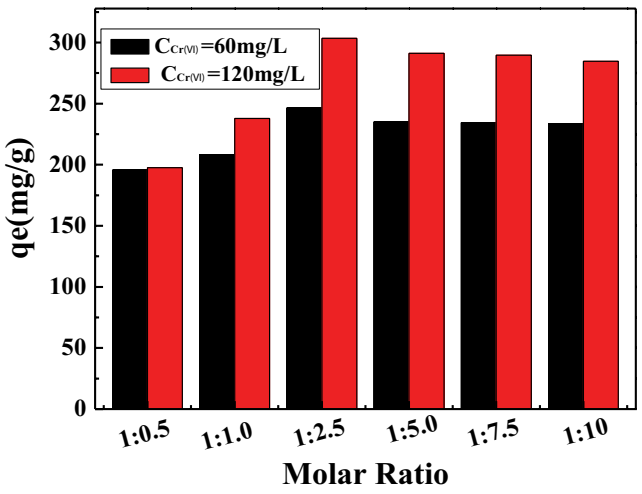

Fig. 8. Effect of the molar ratio of diethylenetriamine (DETA) to cyanuric chloride (CC) on the adsorption of Cr(VI) by GO/CC-DETA.

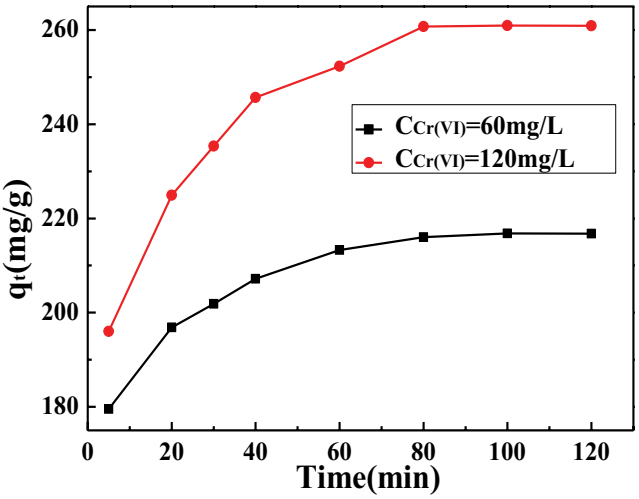

Fig. 9. Effect of contact time on the adsorption of Cr(VI) by GO/CC-DETA.

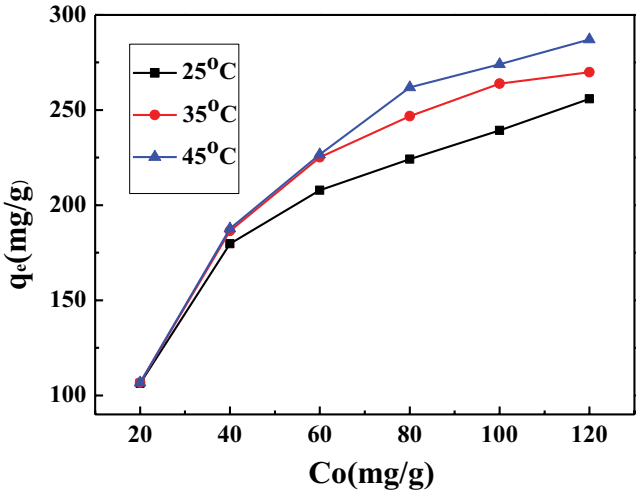

Fig. 10. Effect of contact temperature on the adsorption of Cr(VI) by GO/CC-DETA (5 mg).

in turn controls the residence time of sorbate uptake at the solid–solution interface [31]. The contacting-time curve can obtain the adsorption capacity and equilibrium time, and the fitting parameters of models can reveal the main mechanism controlling the adsorption process. Here, the kinetic adsorption process was pondered to fit five adsorption kinetic models in a linear form.

Pseudo-first-order kinetic model is used to describe the adsorption rate of soluble substances in a solid–liquid system, and the model considers that intraparticle mass transfer resistance is a limiting factor for adsorption [31–33]. Pseudo-second-order kinetic model is based on the assumption that the adsorption rate is controlled by the adsorption reaction at the liquid/solid interface in the adsorbent [31]. Besides, Elovich equation, a rate equation based on adsorption capacity, was employed to distinguish whether the Cr(VI) adsorption process in this work was chemical adsorption or not [34]. Meanwhile, intraparticle diffusion equation was used to analyze the role of diffusion in the control steps of the Cr(VI) adsorption. In order to know whether the actual adsorption process conforms to the pore diffusion model, Bangham equation was also used. And when the kinetics fitted the experimental data in a straight line and passed through the origin, it conveyed that the adsorption process was controlled by the diffusion. On the contrary, the poor linearity would indicate the pore diffusion of adsorbates in adsorbent was not the only rate-limiting step in the adsorption separation, and membrane diffusion and intra-pore diffusion both played important roles in different stages [32]. All model abbreviated formulas are as follows:

Pseudo-first-order kinetic equation [35]:

$$\log(q_e - q_t) = \log q_e - \frac{k_1}{2.303} t \quad (2)$$

Pseudo-second-order kinetic equation [31]:

$$\frac{1}{q_e}t = \frac{t}{q_t} - \frac{1}{k_2 q_e^2} \tag{3}$$

Elovich equation:

$$q_t = \frac{1}{\beta}(\ln \alpha\beta) + \frac{1}{\beta}\ln t \tag{4}$$

Intraparticle diffusion equation:

$$q_t = k_{ip} t^{1/2} + C \tag{5}$$

Bangham equation:

$$\ln q_t = \ln k_b + \frac{1}{m}\ln t \tag{6}$$

where q_e (mg g^{-1}) and q_t (mg g^{-1}) refer to the adsorption amount at time t and the equilibrium state, respectively, and t (min) is the adsorption time; k_1 (min^{-1}), k_2 (g mg^{-1} min^{-1}), α (g mg^{-1} min^{-1}), β (g mg^{-1}), k_{ip} (mg g^{-1} min$^{-0.5}$), C (mg g^{-1}) and k_b (mg g^{-1}) represent the rate constants of the corresponding models. k_2 is related to the initial concentration of the solute, the pH of the solution, the temperature and the stirring conditions. α (g mg^{-1} min^{-1}) is the initial adsorption rate constant and β (g mg^{-1}) is the desorption constant, the calculated q_e in pseudo-second-order kinetic equation is in connection with the extent of surface coverage and activation energy constant for chemisorption. k_{ip} (mg g^{-1} min$^{-0.5}$) is the diffusion rate constant, and constant C (g mg^{-1}) is associated with the influence of boundary layer on adsorption process.

The results of linear fitting and the corresponding kinetic parameters of five kinetic models were presented, respectively (Fig. 11; Table 1). As listed in Table 1, generally speaking, the correlation coefficient values (R^2) were in a decrease order of pseudo-second-order reaction (0.999), Elovich model (0.981), Bangham model (0.977), pseudo-first-order (0.897), intraparticle diffusion model (0.880). Obviously, pseudo-second-order reaction ($R^2 > 0.999$) showed the best relevance which stated the adsorption rate was controlled by chemical process involving electron sharing or electron transfer between adsorbent and adsorbate. Simultaneously, Elovich model equation also had a higher value of the correlation coefficient. Since the Elovich equation is a description of the heterogeneous diffusion process controlled by the reaction rate and diffusion factor, it indicated that the adsorption of Cr(VI) by GO/CC-DETA was a heterogeneous diffusion process, not a simple first-order reaction. The correlation coefficient of the intraparticle diffusion model was smaller. Thus, it was known that internal diffusion was not a control step in the adsorption process.

3.4. Adsorption isotherm

To study the adsorption thermodynamic property of GO/CC-DETA toward Cr(VI), the experimental data were fitted into four isotherms: Langmuir, Freundlich, and Temkin and Dubinin–Radushkevich. Langmuir isotherm model mainly accounts for single-layer adsorption. Besides, its corresponding adsorption process mainly occurs on the outer surface and the adsorption sites are limited, independent and uniformly distributed [36]. Freundlich isotherm model is a modification of the Langmuir isotherm model which considers that the adsorption is reversible, not the monolayer adsorption in the strict sense, and defines the adsorption characteristics for the heterogeneous surface. Temkin isotherm explicitly takes adsorbent–adsorbate interaction into consideration. It assumes the following: (1) it is the interaction force between the adsorbent and the adsorbate that causes the adsorption heat of all molecules on the surface of the adsorbent to decrease linearly with the coverage and (2) The adsorption characteristic is that the binding energy is evenly distributed to reach a certain maximum value [37,38]. Dubinin–Radushkevich isotherm which is based on the theory of micropore filling, considers that the adsorption behavior is a micropore filling process, rather than a surface covering form described by other models. It could be used to determine whether the adsorption process is physical or chemical adsorption [39]. All model formulas are given as follows:
Langmuir isotherm:

$$\frac{C_e}{q_e} = \frac{1}{K_L q_m} + \frac{C_e}{q_m} \tag{7}$$

Freundlich isotherm:

$$\ln q_e = \ln K_F + \frac{1}{n}\ln C_e \tag{8}$$

Temkin isotherm:

$$q_e = \frac{RT}{b_T}\ln C_e + \frac{RT}{b_T}\ln A_T \tag{9}$$

Dubinin–Radushkevich isotherm:

$$\ln q_e = \ln q_s - K_{ad}\varepsilon^2 \tag{10}$$

$$\varepsilon = RT\ln\left(1 + \frac{1}{C_e}\right) \tag{11}$$

$$E = \frac{1}{\sqrt{2K_{ad}}} \tag{12}$$

where C_0 and C_e (mg g^{-1}) are, respectively, the initial and the equilibrium concentration of Cr(VI) and q_e (mg g^{-1}) represents the quantity of target element Cr(VI) adsorbed at equilibrium. R (8.314 J mol^{-1} K^{-1}) and T (K), respectively, represent the gas constant and absolute temperature. q_m (mg g^{-1}) is the theoretical maximum monolayer adsorption capacity of adsorbent material toward Cr(VI). K_L (L mg^{-1}), K_f (mg g^{-1}), A_T (L mg^{-1}), b_T and K_{ad} (mol^2 kJ^{-2}) represent the rate constants of the corresponding models. K_L is a constant associated with the adsorption intensity. q_s (mg g^{-1}) represents the theoretical isotherm saturation capacity.

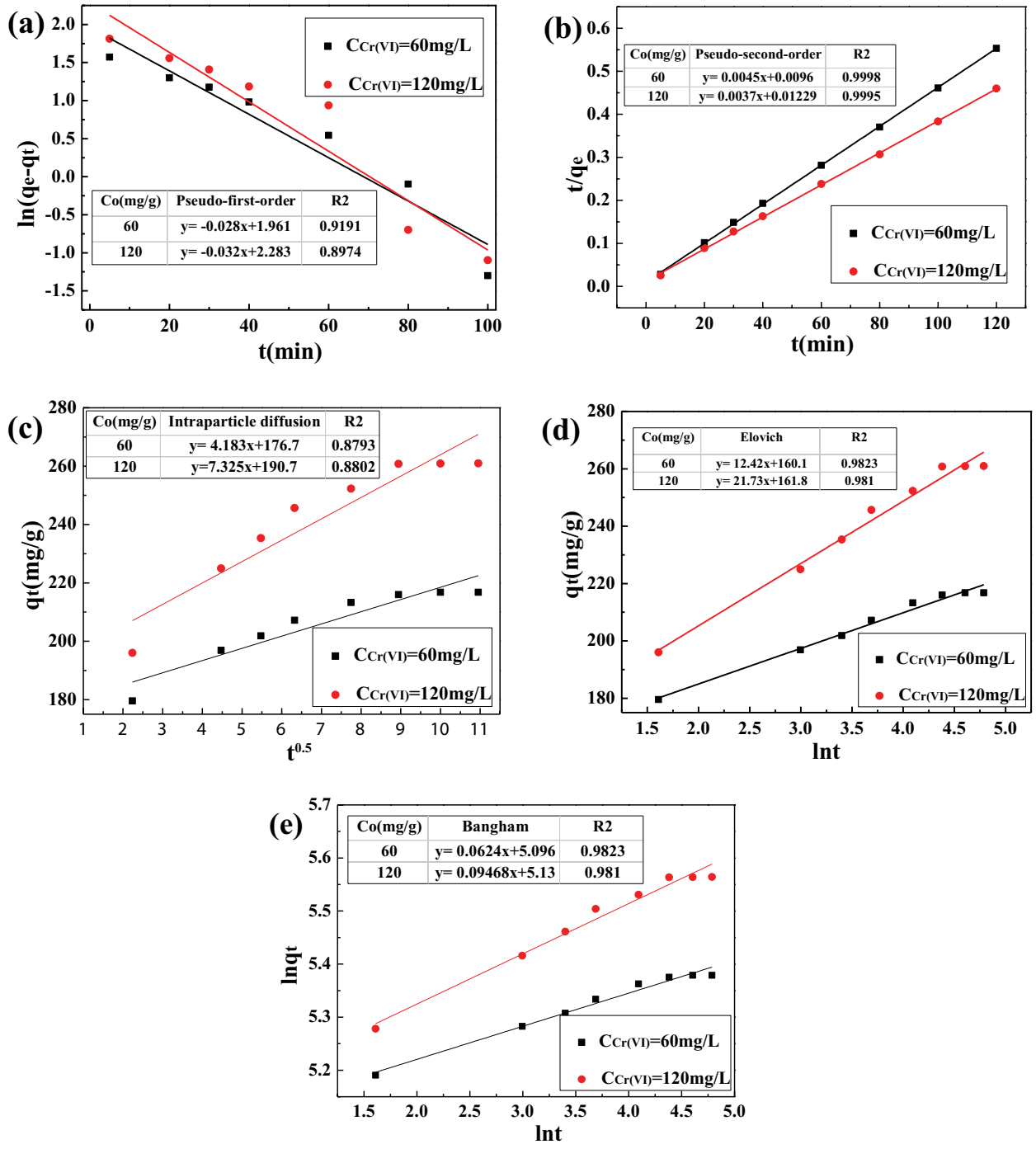

Fig. 11. Five linear kinetic models of Cr(VI) adsorption by GO/CC-DETA: (a) pseudo-first-order, (b) pseudo-second-order, (c) intra-particle diffusion, (d) Elovich, and (e) Bangham.

The constant K_f is an approximate indicator of adsorption capacity, while $1/n$ is a function of the strength of adsorption in the adsorption process. E (kJ mol^{-1}) is the adsorption free energy, and its value can judge the properties of adsorption: ion exchange (8–16 kJ mol^{-1}), physical adsorption (<8 kJ mol^{-1}), chemical adsorption (>16, 20~40 kJ mol^{-1}) [40].

Fitting thermodynamic parameters of above models for experimental temperature adsorption curve (Fig. 10) are listed in Table 2 and their linear fitting results are shown in Fig. 12. By comparing and analyzing these parameters, some optimal models were presented, such as Langmuir isotherm (R^2 = 0.9929–0.9966) and Temkin isotherm (R^2 = 0.9887–0.9970). According to the fitting data from Langmuir isotherm, the maximum monolayer coverage capacity (q_m) was determined to be 257.7–295.9 mg g^{-1} which was close to the practical adsorption equilibrium capacity

Table 1
Kinetic parameters for the adsorption of Cr(VI) onto GO/CC-DETA at room temperature (30°C) and pH = 2

Model	Parameter	Parameter value	
		C_0 = 60 mg L^{-1}	C_0 = 120 mg L^{-1}
Pseudo-first-order	q_e (mg g^{-1})	91.45	191.72
	k_1 (min^{-1})	0.06568	0.07480
	R^2	0.9193	0.8972
Pseudo-second-order	q_e (mg g^{-1})	221.24	268.82
	k_2 (g mg^{-1} min^{-1})	0.002083	0.001128
	R^2	0.9997	0.9995
Elovich model	α (mg mg^{-1} min^{-2})	4.9×10^{-5}	3.7×10^{-4}
	β (g mg^{-1} min^{-1})	0.08050	0.04602
	R^2	0.9823	0.9810
Intraparticle diffusion model	k_{ip} (mg g^{-1} $min^{-0.5}$)	4.183	7.325
	C (mg g^{-1})	176.7	190.7
	R^2	0.8793	0.8802
Bangham model	k_b (mg g^{-1})	163.3	169.9
	m	16.03	10.56
	R^2	0.9798	0.9770

Table 2
Isotherm parameters for the adsorption of Cr(VI) onto GO/CC-DETA at different temperatures at pH = 2

Model	Parameter	Parameter value		
		25°C	35°C	45°C
Langmuir isotherm	q_m (mg g^{-1})	257.7	277.8	295.9
	K_L (L mg^{-1})	0.2834	0.3028	0.2596
	R^2	0.9929	0.9966	0.9951
Freundlich isotherm	n	5.216	4.791	4.531
	K_F (mg g^{-1})	112.2	115.5	4.791
	R^2	0.9765	0.9795	0.9850
Temkin isotherm	b_T	76.70	69.31	65.52
	A_T (L mg^{-1})	29.75	21.36	16.08
	R^2	0.9887	0.9970	0.9942
Dubinin–Radushkevich isotherm	K_{ad} (mol^2 kJ^{-2})	2.2×10^{-7}	2.0×10^{-7}	1.9×10^{-7}
	q_s (mg g^{-1})	222.8	238.0	246.5
	E (kJ mol^{-1})	1,507	2,236	1,622
	R^2	0.8461	0.8395	0.8089

(q_e, 255.9–287.1 mg g^{-1}). This also revealed that it was a monolayer adsorption process and no transmigration of adsorbate in the plane of the surface. Similarly, relatively well-fitted Temkin isotherm (R^2 = 0.9887–0.9970) revealed the existence of adsorbent–adsorbate interaction.

3.5. Adsorption mechanism analysis

Fig. 13 shows that grafted N-rich dendrimer amines GO/CC-DETA nanocomposites could be protonated under aqueous condition and have strong electrostatic interaction with the negatively charged Cr(VI) species, accounting for the excellent adsorption property. Besides, the reduction of Cr(VI) occurred during the adsorption process and there was complexation interaction between the generated Cr(III) and GO/CC-DETA. The obvious Cr2p peak in survey spectra of XPS of GO/CC-$DETA_{Cr\text{-}loaded}$ (Fig. 4a), its N1s XPS spectra (Fig. 4c) and Cr2p XPS spectra (Fig. 4d) proved the adsorption process. The binding of Cr(VI) species on the protonated amine chains triggered the decrease of binding energy of N1s (Fig. 4c). And four peak splits (Fig. 4d) at 588.4, 586.9, 579.3 and 577.2 eV fitted the actual Cr2p peak cure well and the four sub-peaks corresponded to Cr(VI)$2p_{1/2}$, Cr(III)$2p_{1/2}$, Cr(VI)$2p_{3/2}$, Cr(III)$2p3_{1/2}$, respectively [41]. It proved the reduction of Cr(VI).

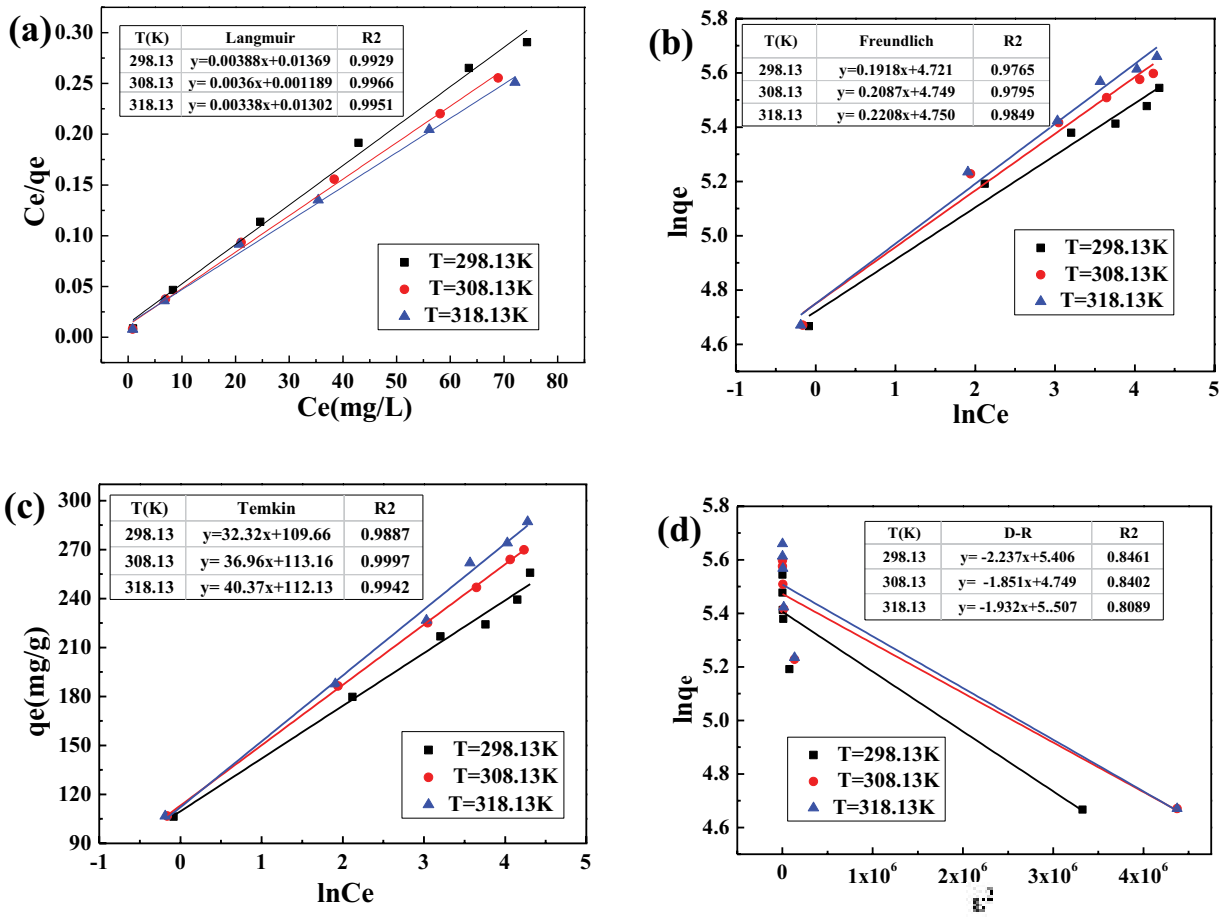

Fig. 12. Linear isothermal models of Cr(VI) adsorption by GO/CC-DETA: (a) Langmuir, (b) Freundlich, (c) Temkin, and (d) Dubinin–Radushkevich (D-R).

To further study the adsorption, the morphology of GO/CC-DETA$_{Cr\text{-}loaded}$ (Fig. 14) is presented. High-resolution TEM images (b,c) and elemental mapping images (a) of GO/CC-DETA$_{Cr\text{-}loaded}$ stated Cr deposition on the GO/CC-DETA and relevant morphology. The initial and residual concentrations of total Cr(VI) were evaluated by ICP-AES. By measuring the concentration of hexavalent chromium in the residual solution after adsorption through ultraviolet spectrophotometry, the amount of trivalent chromium in the residual solution could be known. The result presented the amount of trivalent chromium in the residual solution was almost zero. This indicated that the trivalent chromium produced by the reduction process was almost adsorbed by the material. Due to the protonation easily happening in the acid environment, adsorption capacity increased a lot as pH decreased. It was consistent with the experimental result (Fig. 15).

3.6. Desorption and regeneration study

For the practical application, it was not sufficient with a good adsorption capacity only. Thus, further desorption and regeneration study was indispensable. Obviously, undergoing five cycles, a clear decrease emerged, and a final stable adsorption capacity was reached (~160 mg g^{-1}, Fig. 16).

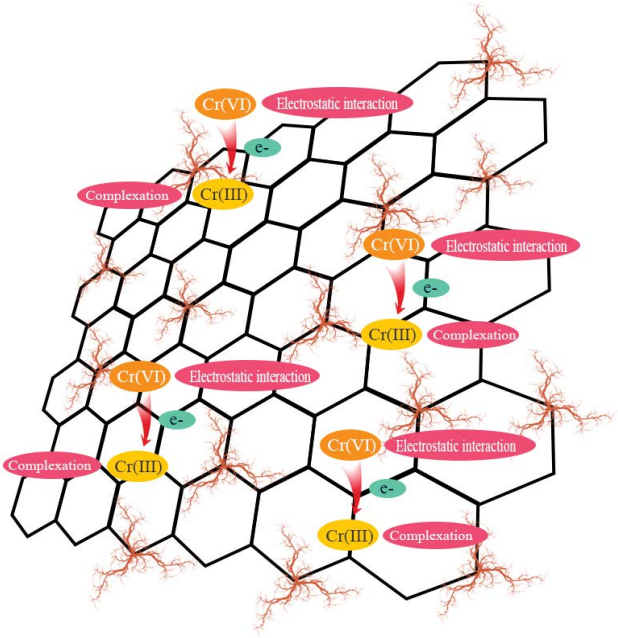

Fig. 13. Schematic representation for adsorption mechanism of Cr(VI) ions by GO/CC-DETA.

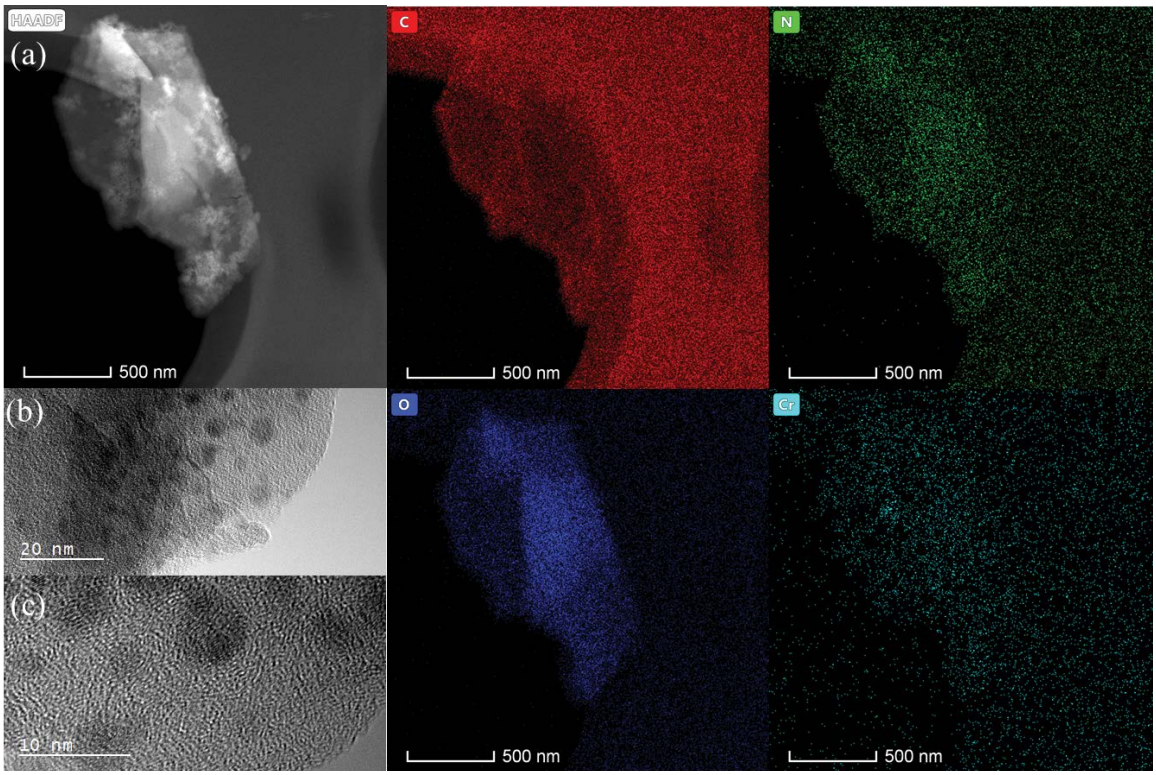

Fig. 14. High-resolution TEM images (b–c) and elemental mapping images (a) of GO/CC-DETA$_{Cr\text{-}loaded}$.

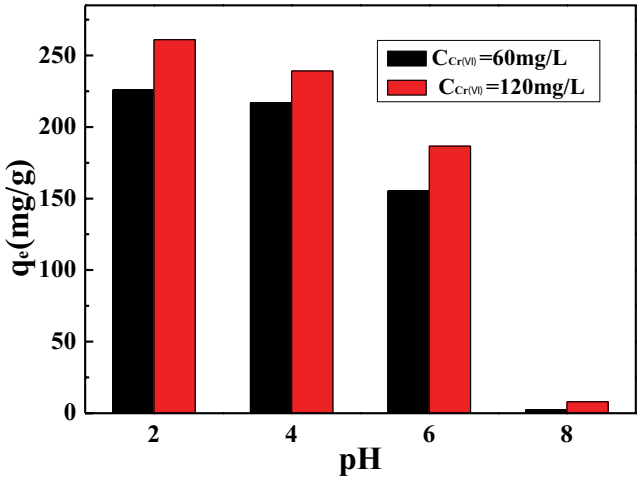

Fig. 15. Effect of solution pH on the adsorption of Cr(VI) by GO/CC-DETA.

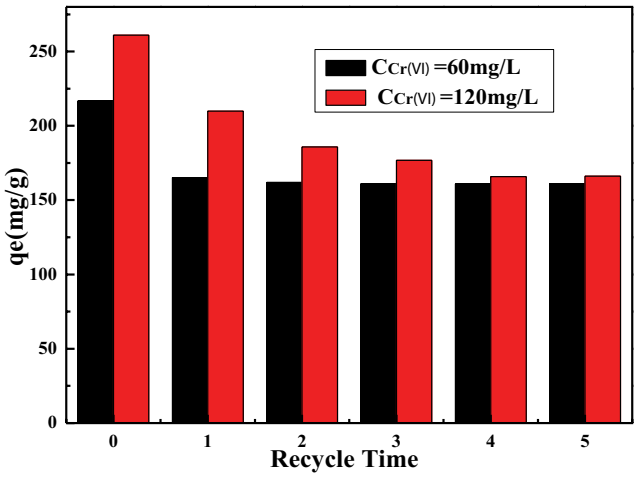

Fig. 16. Reusability of GO/CC-DETA for Cr(VI) adsorption.

The FTIR spectra of GO/CC-DETA, GO/CC-DETA$_{Cr\text{-}loaded}$, GO/CC-DETA$_{desorption}$ (Fig. 2b) presented that the characteristic absorption bands of special groups changed little, where the peaks at 761 cm^{-1} (Cr–O) and 923 cm^{-1} (Cr=O) from chromium were visible. From the embedded figure in Fig. 4a, it was known that part of adsorbed Cr was preserved. High-resolution TEM images (Figs. 14b and c) of GO/CC-DETA$_{desorption}$ illustrated the residual, where many black dots with a diameter of 1–5 nm were discovered. And elemental mapping images (Fig. 2a) of GO/CC-DETA$_{desorption}$ assisted in presenting the elemental analysis. It was concluded that some adsorbed Cr occupied adsorption sites and was hard to elute out which explained the loss of adsorption capacity. Notwithstanding, the adsorption property of GO/CC-DETA deserved recognition and was still valuable.

4. Conclusions

In the present study, N-rich dendrimer amines grafted onto graphene oxide (GO/CC-DETA) was successfully developed for the removal of Cr(VI) ions from aqueous solution.

The adsorption studies of optimal molar ratio, pH, contact time, and temperature were carried out in batch mode, and the prepared GO/CC-DETA with a 1:2.5 molar ratio of DETA to CC performed the best result at pH = 2. The adsorption equilibrium was reached in about 80 min, and hyperthermal surrounding favored the adsorption process. Langmuir isotherm model and the pseudo-second-order kinetic model were found applicable in terms of relatively high regression values. The maximum monolayer adsorption capacity of the GO/CC-DETA, as obtained from the Langmuir adsorption isotherm, was found to be 295.9 mg g^{-1}. And the main adsorption mechanism of GO/CC-DETA toward Cr(VI) was electrostatic interaction. The desorption–regeneration results showed that the adsorption capacity could remain relatively stable after several times of usage. Thus, GO/CC-DETA deserved to be recognized as a promising adsorbent for the removal of Cr(VI) ions from aqueous solution.

Acknowledgements

This work was supported by the Educational and Teaching Research and Reform Projects of Guangdong Provincial Education Department ([2018]180).

References

[1] S. Jaison, T. Muthukumar, Chromium accumulation in medicinal plants growing naturally on tannery contaminated and non-contaminated soils, Biol. Trace Elem. Res., 175 (2017) 223–235.
[2] M. Shahid, S. Shamshad, M. Rafiq, S. Khalid, I. Bibi, N.K. Niazi, C. Dumat, M.I. Rashid, Chromium speciation, bioavailability, uptake, toxicity and detoxification in soil-plant system: a review, Chemosphere, 178 (2017) 513–533.
[3] F. Noli, P. Tsamos, Concentration of heavy metals and trace elements in soils, waters and vegetables and assessment of health risk in the vicinity of a lignite-fired power plant, Sci. Total Environ., 563 (2016) 377–385.
[4] International Agency for Research on Cancer, Overall evaluations of Carcinogenicity: An Updating in IARC Monographs, Vols. 1–42, IARC Monographs on the Evaluation of Carcinogenic Risks to Humans – Overall Evaluations of Carcinogenicity: An Updating of IARC Mongraphs, 1987.
[5] Y. Xing, X. Chen, D. Wang, Electrically regenerated ion exchange for removal and recovery of Cr(VI) from wastewater, Environ. Sci. Technol., 41 (2007) 1439–1443.
[6] R. Gayathri, P. Senthil Kumar, Recovery and reuse of hexavalent chromium from aqueous solutions by a hybrid technique of electrodialysis and ion exchange, Braz. J. Chem. Eng., 27 (2010) 71–78.
[7] A.K. Bhattacharya, T.K. Naiya, S.N. Mandal, S.K. Das, Adsorption, kinetics and equilibrium studies on removal of Cr(VI) from aqueous solutions using different low-cost adsorbents, Chem. Eng. J., 137 (2008) 529–541.
[8] P. Miretzky, A.F. Cirelli, Cr(VI) and Cr(III) removal from aqueous solution by raw and modified lignocellulosic materials: a review, J. Hazard. Mater., 180 (2010) 1–19.
[9] A.K. Golder, A.K. Chanda, A.N. Samanta, S. Ray, Removal of hexavalent chromium by electrochemical reduction–precipitation: investigation of process performance and reaction stoichiometry, Sep. Purif. Technol., 76 (2011) 345–350.
[10] C. Blöcher, J. Dorda, V. Mavrov, H. Chmiel, N.K. Lazaridis, K.A. Matis, Hybrid flotation—membrane filtration process for the removal of heavy metal ions from wastewater, Water Res., 37 (2003) 4018–4026.
[11] J.-M. Sun, C. Shang, J.-C. Huang, Co-removal of hexavalent chromium through copper precipitation in synthetic wastewater, Environ. Sci. Technol., 37 (2003) 4281–4287.
[12] B.A. Marinho, R.O. Cristóvão, R. Djellabi, J.M. Loureiro, R.A.R. Boaventura, V.J.P. Vilar, Photocatalytic reduction of Cr(VI) over TiO_2-coated cellulose acetate monolithic structures using solar light, Appl. Catal., B, 203 (2017) 18–30.
[13] A.M. Yusof, N.A. Malek, Removal of Cr(VI) and As(V) from aqueous solutions by HDTMA-modified zeolite Y, J. Hazard. Mater., 162 (2009) 1019–1024.
[14] A. Abhishek, N. Saranya, P. Chandi, N. Selvaraju, Studies on the remediation of chromium(VI) from simulated wastewater using novel biomass of *Pinus kesiya* cone, Desal. Wat. Treat., 114 (2018) 192–204.
[15] N. Saranya, A. Ajmani, V. Sivasubramanian, N. Selvaraju, Hexavalent chromium removal from simulated and real effluents using *Artocarpus heterophyllus* peel biosorbent - Batch and continuous studies, J. Mol. Liq., 265 (2018) 779–790.
[16] D. Park, J.M. Park, Y.-S. Yun, Mechanisms of the removal of hexavalent chromium by biomaterials or biomaterial-based activated carbons, J. Hazard. Mater., 137 (2006) 1254–1257.
[17] H. Fida, S. Guo, G. Zhang, Preparation and characterization of bifunctional Ti–Fe kaolinite composite for Cr(VI) removal, J. Colloid Interface Sci., 103 (2018) 113–121.
[18] X. Jin, M. Jiang, J. Du, Z. Chen, Removal of Cr(VI) from aqueous solution by surfactant-modified kaolinite, J. Ind. Eng. Chem., 20 (2014) 3025–3032.
[19] A.H. Qusti, Removal of chromium(VI) from aqueous solution using manganese oxide nanofibers, J. Ind. Eng. Chem., 20 (2014) 3394–3399.
[20] S. Rengaraj, K.-H. Yeon, S.-H. Moon, Removal of chromium from water and wastewater by ion exchange resins, J. Hazard. Mater., 87 (2001) 273–287.
[21] Z. Wang, J. Yang, Y. Li, Q. Zhuang, J. Gu, Simultaneous degradation and removal of Cr^{VI} from aqueous solution with Zr-based metal–organic frameworks bearing inherent reductive sites, Chem. Eur. J., 23 (2017) 15415–15423.
[22] Z. Wang, J. Yang, Y. Li, Q. Zhuang, J. Gu, In situ carbothermal synthesis of nanoscale zero-valent iron functionalized porous carbon from metal-organic frameworks for efficient detoxification of chromium(VI), Eur. J. Inorg. Chem., 2018 (2018) 23–30.
[23] X. Feng, C. Liang, J. Yu, X. Jiang, Facile fabrication of graphene oxide-polyethylenimine composite and its application for the Cr(VI) removal, Sep. Sci. Technol., 53 (2018) 2376–2387.
[24] Y. Wu, H. Luo, H. Wang, C. Wang, J. Zhang, Z. Zhang, Adsorption of hexavalent chromium from aqueous solutions by graphene modified with cetyltrimethylammonium bromide, J. Colloid Interface Sci., 394 (2013) 183–191.
[25] A.S.K. Kumar, S.S. Kakan, N. Rajesh, A novel amine impregnated graphene oxide adsorbent for the removal of hexavalent chromium, Chem. Eng. J., 230 (2013) 328–337.
[26] D.D. Maksin, A.B. Nastasović, A.D. Milutinović-Nikolić, L.T. Suručić, Z.P. Sandić, R.V. Hercigonja, A.E. Onjia, Equilibrium and kinetics study on hexavalent chromium adsorption onto diethylene triamine grafted glycidyl methacrylate based copolymers, J. Hazard. Mater., 209 (2012) 99–110.
[27] H. Li, S. Bi, L. Liu, W. Dong, X. Wang, Separation and accumulation of Cu(II), Zn(II) and Cr(VI) from aqueous solution by magnetic chitosan modified with diethylenetriamine, Desalination, 278 (2011) 397–404.
[28] R. Zhao, X. Li, B. Sun, H. Ji, C. Wang, Diethylenetriamine-assisted synthesis of amino-rich hydrothermal carbon-coated electrospun polyacrylonitrile fiber adsorbents for the removal of Cr(VI) and 2,4-dichlorophenoxyacetic acid, J. Colloid Interface Sci., 487 (2017) 297–309.
[29] A. Misra, P.K. Tyagi, M.K. Singh, D.S. Misra, FTIR studies of nitrogen doped carbon nanotubes, Diamond Relat. Mater., 15 (2006) 385–388.
[30] H.-P. Cong, X.-C. Ren, P. Wang, S.-H. Yu, Macroscopic multifunctional graphene-based hydrogels and aerogels by a metal ion induced self-assembly process, ACS Nano, 6 (2012) 2693–2703.
[31] Y.S. Ho, G. McKay, Pseudo-second order model for sorption processes, Process Biochem., 34 (1999) 451–465.
[32] S. Nethaji, A. Sivasamy, A.B. Mandal, Preparation and characterization of corn cob activated carbon coated with

nano-sized magnetite particles for the removal of Cr(VI), Bioresour. Technol., 134 (2013) 94–100.
[33] D. Duranoğlu, A.W. Trochimczuk, U. Beker, Kinetics and thermodynamics of hexavalent chromium adsorption onto activated carbon derived from acrylonitrile-divinylbenzene copolymer, Chem. Eng. J., 187 (2012) 193–202.
[34] C.W. Cheung, J.F. Porter, G. McKay, Sorption kinetics for the removal of copper and zinc from effluents using bone char, Sep. Purif. Technol., 19 (2000) 55–64.
[35] Z. Aksu, Biosorption of reactive dyes by dried activated sludge: equilibrium and kinetic modelling, Biochem. Eng. J., 7 (2001) 79–84.
[36] A.O. Dada, A.P. Olalekan, A.M. Olatunya, O. Dada, Langmuir, Freundlich, Temkin and Dubinin–Radushkevich isotherms studies of equilibrium sorption of Zn^{2+} unto phosphoric acid modified rice husk, IOSR J. Appl. Chem., 3 (2012) 38–45.
[37] D. Kavitha, C. Namasivayam, Experimental and kinetic studies on methylene blue adsorption by coir pith carbon, Bioresour. Technol., 98 (2007) 14–21.
[38] I.D. Mall, V.C. Srivastava, N.K. Agarwal, I.M. Mishra, Removal of congo red from aqueous solution by bagasse fly ash and activated carbon: kinetic study and equilibrium isotherm analyses, Chemosphere, 61 (2005) 492–501.
[39] I. Kiran, T. Akar, A.S. Ozcan, A. Ozcan, S. Tunali, Biosorption kinetics and isotherm studies of Acid Red 57 by dried *Cephalosporium aphidicola* cells from aqueous solutions, Biochem. Eng. J., 31 (2006) 197–203.
[40] D. Aggarwal, M. Goyal, R.C. Bansal, Adsorption of chromium by activated carbon from aqueous solution, Carbon, 37 (1999) 1989–1997.
[41] D. Park, Y.-S. Yun, H.W. Lee, J.M. Park, Advanced kinetic model of the Cr(VI) removal by biomaterials at various pHs and temperatures, Bioresour. Technol., 99 (2008) 1141–1147.